PERGAMON

International Journal of Solids and Structures 38 (2001) 3877–3904

INTERNATIONAL JOURNAL OF SOLIDS and STRUCTURES

www.elsevier.com/locate/ijsolstr

A structural approach of plastic microbuckling in long fibre composites: comparison with theoretical and experimental results

S. Drapier [a,*], J.-C. Grandidier [b], M. Potier-Ferry [c]

[a] *Department of Mechanical and Materials Engineering, ÉNS des Mines de Saint-Étienne, 42023 Saint-Étienne Cedex 02, France*
[b] *L3MA-SP2MI, Téléport 2, boulevard Pierre et Marie Curie, BP30179, 86962 Futuroscope Chasseneuil Cedex, France*
[c] *Laboratoire de Physique et Mécanique des Matériaux, ISGMP, Île du Saulcy, 57045 Metx Cedex 02, France*

Received 24 January 2000

Abstract

The aim of this paper is to compare some predictions obtained from a structural plastic microbuckling model presented in detail by Drapier et al. (1999), with theoretical and experimental results from the literature. After a short presentation of this model, it is established that with our approach it is possible to find the elastic modes determined by Drapier et al. (1996) on the composite microstructure. The plastic instability mechanism is then investigated and its understanding is refined. Some simulations are carried out varying the fibre initial imperfection, and the results are detailed and compared with predictions from a kink-band model (Budiansky and Fleck, 1993). Compared to the present knowledge, the understanding of the influence of the imperfection shape and of its distribution across the ply thickness is improved and new results are exposed. Validation of the present approach is completed by comparing the influence of both matrix and fibre behaviours as predicted by Budiansky and Fleck (1993) with the ones obtained from our numerical tool. Results demonstrate the influence of the change in the matrix tangent stiffness.

Secondly, we have quantified the effects of the applied loading, thickness and stacking sequence on the compressive strength of laminates. Numerical predictions provide new results that yield a proper justification of the very high compressive strength measured with bending tests. These predictions also fit well experimental measurements from the literature showing the effects of the thickness (Wisnom, 1992) and of the stacking sequence (Grandsire-Vinçon, 1993) on the compressive strength. For the first time, the effect of the gradient of loading across the laminate thickness is predicted. Results are shown to correlate well with experimental results from Wisnom et al. (1997).

Keywords: Compression; Long-fibre composites; Non-linear plastic microbuckling; Mesoscopic model; Structural effects

* Corresponding author. Tel.: +33-04-77420079; fax: +33-04-77420249.
E-mail addresses: drapier@emse.fr (S. Drapier), jcg@13ma.univ-poitiers.fr (J.-C. Grandidier), potier-ferry@lpmm.univ-metz.fr (M. Potier-Ferry).

0020-7683/01/$ - see front matter
PII: S0020-7683(00)00247-X

1. Introduction

Characterising and predicting the compressive strength of long-fibre composites originated lots of papers. It is now well established that failure is initiated by a fibre instability called microbuckling (Rosen, 1964) that leads to the catastrophic formation of a kink-band (Argon, 1972; Budiansky, 1983). The main parameters that influence this mechanism are the matrix physical non-linearity and the presence of fibre initial wavy imperfections. The most comprehensive models proposed in the literature very well account for these effects. For instance, Budiansky and Fleck (1993) starting from a kink-band model gave a simple expression of the compressive stress at failure corresponding to an increase in the kink-band rotation:

$$\sigma_c = \frac{G}{1 + n\left(\frac{3}{7}\right)^{1/n}\left(\frac{\bar{\phi}/\gamma_y^c}{n-1}\right)^{(n-1)/n}}, \tag{1}$$

where G is the elastic shear modulus of the composite and $\bar{\phi}$ is the initial inclination angle of the kink band. In this work, the non-linear response of the matrix is modelled through a constitutive law of Ramberg–Osgood's type whose strain hardening coefficient is denoted by n and yield strain in shear is γ_y^c. These authors compared some predictions given by expression (1) with some experimental results measured in various pure compressive tests. It is clear that amplitudes of the initial wavy imperfection and mechanical characteristics of the matrix that lead to a good correlation with the experimental results have both realistic values.

Despite their efficiency, the kink-band models cannot provide any explanation to the high strength of unidirectional plies measured with bending devices. As an example, under a bending loading T300/914 unidirectional plies can withstand compressive strains greater than 2%, whereas under a pure compression loading, this strength is lower than 1.2% (t'Hart et al., 1991). This observation can lead to hypothesis that pure compression tests yield a very poor estimation of the compressive strength, as suggested by the results from t'Hart et al. (1991). Recently, Anthoine et al. (1998) demonstrated, thanks to a numerical simulation, that even from a theoretical point of view, it is really difficult to set up pure compression tests on thin laminates. Then, the comparison with experimental results presented in many papers must be examined cautiously. Without questioning the dispersive character of pure compression tests observed experimentally, one can postulate that the local plastic microbuckling instability is influenced by the structure at the ply scale. This hypothesis is verified experimentally by several experimental works (Wisnom, 1991, 1992; Grandidier et al., 1992; Colvin and Swanson, 1993; Grandsire-Vinçon, 1993; Wisnom et al., 1997), which demonstrate the effect of the stacking sequence, loading and ply thickness on the resulting compressive strength.

The influence of these structural parameters on failure can be tackled by discretising the whole microstructure of the ply. For instance, Drapier et al. (1996) have clearly established by this way the influence of the ply thickness, loading and stacking sequence on the elastic microbuckling modes. On the basis of a heterogeneous bidimensional representation, Kyriakides et al. (1995) described the complete process of the microbuckling occurrence followed by a kink-band formation. However, the large number of degrees of freedom that is required in a discretisation of the whole ply does not allow us to account for the influence of the structural parameters on the failure. Conversely, this can be avoided if the microstructural behaviour is represented through an homogeneous equivalent medium (HEM) that efficiently accounts for the fibre bending, as shown by Grandidier et al. (1992) and Fleck et al. (1995a).

Thanks to homogeneous models of plies several authors (Schaffers, 1977; Swanson, 1992; Grandidier and Potier-Ferry, 1990; Grandidier et al., 1992) investigated the instability at the scale of unidirectional plies. The microbuckling amplitude is sought as a function of both the fibre position across the thickness and the boundary conditions prescribed on the two faces of the ply in which the instability takes place. These structural models establish clearly the major role of the transverse characteristic length along with

the fibre bending. In most of these works, the change of the solution across the thickness, which depends on structural data, is given a priori. More recently, Drapier et al. (1999) proposed a homogenised model including the fibre bending and was able to represent the effect of both fibre initial imperfection and matrix non-linear behaviour. The strongly non-linear development of the instability across the whole ply thickness is simulated numerically thanks to a specific finite element whose interest is to reduce largely the computation efforts. This model and the numerical resolution associated with are detailed in Drapier et al. (1999), where many simulations showed that the structural parameters must be taken into account, in the same manner as the imperfection and the matrix plasticity are. These computations permitted for the first time to demonstrate the influence on plastic microbuckling, of the loading (bending or compression), of the ply thickness, and the location of the ply in the laminate (on the edge or between cross-plies). A qualitative comparison with experimental results of the literature has been proposed and the high strength obtained under bending has been explained.

However, with the aim of making this work complete, we want to compare quantitatively the predictions obtained from this model with bending and compression test results carried out on unidirectional (UD) plies and laminates. Moreover, it is necessary to validate this method by comparing the predictions from our approach with others from the literature.

After a short presentation of our model, its ability to grasp the elastic modes is established by comparing them with the modes determined by Drapier et al. (1997). Then the role of the initial imperfection and the influence of the mechanical characteristics on the microbuckling mechanism is then detailed. The very low computation requirements enable one to demonstrate the effect of the initial imperfection shape along with its spatial distribution. The influence of both the fibre initial imperfection and the matrix non-linearity is presented and compared with the trends provided by the kink-band model of Budiansky and Fleck (1993). Eventually, a comparison with the experimental results demonstrate the ability of the present model to capture the effect of the structural parameters on the compressive strength of laminates observed experimentally. The various results confirm the necessity to account for these structural parameters in predicting the compressive strength of laminates. They also improve the understanding of the plastic microbuckling phenomenon.

2. A structural plastic microbuckling model

The equations of the problem and the numerical model are presented in Drapier et al. (1999) which the reader should refer to for technical details. The idea underlying this model is to have the stress and strain at failure (when microbuckling occurs) with very small amounts of computations while taking into account precisely all the parameters governing the phenomenon: size and shape of the initial imperfection, stiffness drop associated with the matrix plastic behaviour, and structural data across the plate thickness (thickness, bending or compression loading, stacking sequence). For further computation reductions, this model is limited to the moderate rotation framework and therefore, aims only at determining the response of laminates up to the occurrence of plastic microbuckling.

2.1. Formulation of the mesoscopic problem

In this model, only compression and bending loadings are considered. A bidimensional representation of a laminate is used (Fig. 1), where $\mathbf{e}_1$ is the 0° direction corresponding to the loading direction. In what follows, derivatives with respect to the fibre direction are denoted as $X' = \partial X/\partial x_1$ and $X'' = \partial^2 X/\partial x_1^2$.

Displacement along $\mathbf{e}_1$ is $u(\mathbf{x})$ and displacement along $\mathbf{e}_2$ is $v(\mathbf{x})$. Stresses (second Piola–Kirchhoff tensor) are denoted as $\mathbf{S}$ and Green–Lagrange's strain tensor is $\boldsymbol{\gamma}$. Based on the works of Grandidier et al. (1992), a

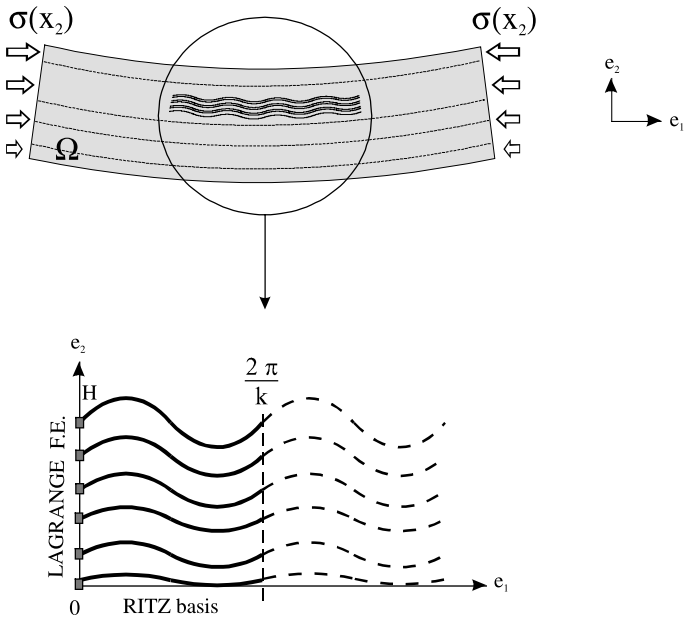

Fig. 1. Bidimensional domain studied.

formulation of the plastic microbuckling problem can be proposed where the virtual works developed in any virtual displacement field $\delta\mathbf{u}(\mathbf{x})$ is given as follows (2):

$$-\int_{\Omega}\left\{fE_{\mathrm{f}}r_{\mathrm{gf}}^{2}v''\delta v''+\mathbf{S}\cdot\delta\boldsymbol{\gamma}\right\}\mathrm{d}\Omega+\langle\mathbf{F},\delta\mathbf{u}\rangle=0\quad\forall\,\delta\mathbf{u}, \tag{2}$$

where f is the fibre volume fraction, E_{f}, the fibre Young modulus and r_{gf}, the fibre gyration radius. $\mathbf{F}$ represents the external loading, and the corresponding virtual work is assumed to depend linearly on the virtual displacement field through the scalar product noted $\langle,\rangle$.

The constitutive law (3) is of anisotropic type, the secant modulus tensor $\mathbf{L}$ being obtained from explicit homogenisation formulas based upon the constituents behaviour (Gardin and Potier-Ferry, 1992). Plasticity is defined at the microscopic scale to describe simply the anisotropy induced by fibre microbuckling. Then, only the matrix material is non-linear and follows an isotropic law of J2 deformation type that yields good predictions of plastic buckling (Hutchinson, 1974):

$$\mathbf{S}(\boldsymbol{\gamma})=\mathbf{L}(\boldsymbol{\gamma})\cdot\boldsymbol{\gamma}. \tag{3}$$

This medium is not classical due to the first term of Eq. (2) which represents the fibre bending energy. This is essential in predicting the effect of the structural data (Gardin and Potier-Ferry, 1992; Drapier et al., 1999) and also to predict the microbuckling wavelength (Grandidier et al., 1992). The micropolar medium was also presented by Fleck and Shu (1995b) and differs mainly by the constitutive law and choice of moderate rotations. The presence of this bending term has been justified by a homogenisation study using the multi-scale method (Gardin and Potier-Ferry, 1992) and also by comparing modes and buckling loads from this approach with micro-heterogeneous modelling results (Drapier et al., 1996). In the case of a laminate, this effect of the fibre bending will be taken into account only in 0° plies. In the other plies, the equivalent behaviour will be calculated from a classical rule of mixtures.

Considering mainly uniaxial loadings, non-linear terms in the strain tensor are reduced to the terms in the loading direction. The fibre initial misalignment is represented through a 'deflection field' $v_0(\mathbf{x})$ defining the fibre initial position in the domain Ω. Then, the strain tensor is given as follows (Eq. 4):

$$\boldsymbol{\gamma}(\mathbf{u}) = \boldsymbol{\varepsilon}(\mathbf{u}) + \boldsymbol{\gamma}(\mathbf{u})_{11}^{\mathrm{NL}}\ \mathbf{e}_1 \otimes \mathbf{e}_1$$
$$\text{with}\quad \boldsymbol{\varepsilon}(\mathbf{u}) = \begin{pmatrix} \frac{\partial u}{\partial x_1} & \frac{1}{2}\left(\frac{\partial u}{\partial x_2} + \frac{\partial v}{\partial x_1}\right) \\ \frac{1}{2}\left(\frac{\partial u}{\partial x_2} + \frac{\partial v}{\partial x_1}\right) & \frac{\partial v}{\partial x_2} \end{pmatrix} \text{ and } \boldsymbol{\gamma}(\mathbf{u})_{11}^{\mathrm{NL}} = \frac{1}{2}\left(\frac{\partial v}{\partial x_1}\right)^2 + \frac{\partial v}{\partial x_1}\frac{\partial v_0}{\partial x_1}. \tag{4}$$

2.2. Mesoscopic formulation of the microbuckling problem

Usually a numerical approach can be deduced from the continuous formulation through an adequate discretisation. In the present case, a further refinement is introduced which leads to a tractable model. Indeed, the microbuckling and imperfection wavelengths are of the order of some hundreds of micrometers, which is comparable to the ply thickness but much smaller than the size of composite structures. Then, a double-scale kinematics is introduced to represent at the ply scale this local short-wavelength phenomenon. The solution of the microbuckling problem is sought under the form of a displacement field (5) evolving at the scale of the structure (denoted $\mathbf{u}_{\mathrm{G}}$), very locally modulated by a displacement field evolving at the ply scale (denoted $\mathbf{u}_{\mathrm{L}}$),

$$\mathbf{u}(\mathbf{x}) = \mathbf{u}_{\mathrm{G}}(\mathbf{x}) + \mathbf{u}_{\mathrm{L}}(\mathbf{x}). \tag{5}$$

With the hypothesis of quick variations of $\mathbf{u}_{\mathrm{L}}$ and slow variations of $\mathbf{u}_{\mathrm{G}}$, the strain tensor can be simplified (Eq. 6) as:

$$\boldsymbol{\gamma}(\mathbf{u}) = \boldsymbol{\gamma}_{\mathrm{G}}(\mathbf{u}_{\mathrm{G}}) + \boldsymbol{\gamma}_{\mathrm{L}}(\mathbf{u}_{\mathrm{L}}),$$
$$\text{with}\quad \begin{cases} \boldsymbol{\gamma}_{\mathrm{G}}(\mathbf{u}_{\mathrm{G}}) = \boldsymbol{\varepsilon}(\mathbf{u}_{\mathrm{G}}) + \left(\frac{v_{\mathrm{G}}'^2}{2}\right)\mathbf{e}_1 \otimes \mathbf{e}_1 \\ \boldsymbol{\gamma}_{\mathrm{L}}(\mathbf{u}_{\mathrm{L}}) = \boldsymbol{\varepsilon}(\mathbf{u}_{\mathrm{L}}) + \left(\frac{v_{\mathrm{L}}'^2}{2} + v_{\mathrm{L}}' v_0'\right)\mathbf{e}_1 \otimes \mathbf{e}_1. \end{cases} \tag{6}$$

With these approximations (4) and (6) and assuming that the displacement $\mathbf{u}_{\mathrm{G}}$ is a known solution of the equilibrium equations (2) and (3), one gets the variational equation describing the mesoscopic equilibrium, the solution of which is $\mathbf{u}_{\mathrm{L}}(\mathbf{x})$ (Eq. (7)):

$$\int_{\Omega} \{f E_{\mathrm{f}} r_{\mathrm{gf}}^2 v_{\mathrm{L}}'' \delta v_{\mathrm{L}}'' + \mathbf{S}_{\mathrm{L}}(\boldsymbol{\gamma}_{\mathrm{G}}, \boldsymbol{\gamma}_{\mathrm{L}}) \cdot \delta\boldsymbol{\gamma}_{\mathrm{L}} + S_{11}(\boldsymbol{\gamma}_{\mathrm{G}})(v_{\mathrm{L}}' + v_0')\delta v_{\mathrm{L}}'\} \mathrm{d}\Omega = 0 \quad \forall \delta\mathbf{u}_{\mathrm{L}}, \tag{7}$$

where $\mathbf{S}_{\mathrm{L}}(\boldsymbol{\gamma}_{\mathrm{G}}, \boldsymbol{\gamma}_{\mathrm{L}}) = \mathbf{S}(\boldsymbol{\gamma}_{\mathrm{G}} + \boldsymbol{\gamma}_{\mathrm{L}}) - \mathbf{S}(\boldsymbol{\gamma}_{\mathrm{G}})$.

One may notice that in this mesoscopic formulation (7), the external loading no longer appears and is replaced by the global field through the global strain tensor $\boldsymbol{\gamma}_{\mathrm{G}}(\mathbf{u}_{\mathrm{G}})$ (Eq. (6). In order to simplify the problem, the global strain tensor is limited to its axial component (8), corresponding to a global displacement induced by compression or bending-compression states:

$$\boldsymbol{\gamma}_{\mathrm{G}}(x_2) = \gamma_{\mathrm{G}11}(x_2)\mathbf{e}_1 \otimes \mathbf{e}_1. \tag{8}$$

2.3. Displacement approximation

As we aim at the greatest efficiency, the number of degrees of freedom has to be minimum. In the framework of cellular instabilities, the displacement field approximation is chosen as a product of

amplitude across the ply thickness with few Ritz basis functions in the fibre direction. This hypothesis also allows for a reduction of the bidimensional mesoscopic domain Ω studied to a single wavelength in the fibre direction (Fig. 1), greatly reducing the amount of computations.

Ritz basis functions are selected so that microbuckling elastic modes obtained by Drapier et al. (1996) can be reproduced, and that a quasi-constant buckling stress can be obtained. Let us notice that the hypothesis of buckling with a constant stress is classical for slender structures. Eventually, the displacement approximation is (9):

$$\mathbf{u}(\mathbf{x}) = \begin{cases} U_1(x_2)\cos(kx_1) + U_2(x_2)\sin(2kx_1), \\ V_1(x_2)\sin(kx_1) + V_2(x_2)\sin(3kx_1), \end{cases} \tag{9}$$

where k is the wavenumber and functions $U_i(x_2)$, $V_i(x_2)$ are the magnitudes of the displacement field which are discretised by a three-noded finite element of Lagrange type (Fig. 1). The imperfection is assumed to have a similar form. Here it is considered as a combination of two sinusoids with a variable amplitude $(V_{01}(x_2), V_{02}(x_2))$ across the thickness and with wavelengths of k and $3k$ respectively (10):

$$v_0(\mathbf{x}) = V_{01}(x_2)\sin(kx_1) + V_{02}(x_2)\sin(3kx_1). \tag{10}$$

There is thus no limitation in describing the change in the displacement fields and the imperfection across the laminate thickness. This is important in order to account for the influence of the structural parameters. Conversely, the Ritz approximation in the axial direction is more restrictive and this is what limits a proper representation of the localisation of the instability. Representing both localisation in the fibre direction and structure effect across the thickness would require a too large model. Consequently, the model focuses on the response up to the maximum load corresponding to the instability occurrence.

2.4. Elastic modes

In order to validate our approach of microbuckling, elastic computations have been carried out on UD plies. The mechanical characteristics are similar to the ones used by Drapier et al. (1996) and correspond to a T300/914 material (Table 1). The imperfection is chosen as constant across the thickness and its wavelength is 0.63 mm ($k = 0.01$). In Fig. 2 are represented, versus the prescribed strain, the change in the transverse displacement of a fibre located at the three fourth of the 1.6 mm ply thickness. The various lines correspond to plies whose amplitude V_{01} varies from 0.1 to 7 μm, whereas V_{02} is null. One can notice that the smaller the amplitude, the closer the response from the fundamental microbuckling path. In Fig. 3, one can observe that for these small amplitude values the displacement field distribution across the thickness is similar to the one obtained by Drapier et al. (1996) who characterised the elastic microbuckling mode by discretising the whole microstructure of the ply. The boundary layer observed close to a free face (top face here) is properly represented by our homogenised model. These results demonstrate the ability of our model

Table 1
Characteristics of T300/914 material and data used by default for the microbuckling mechanism study (Section 3)

Fibre T300 (isotropic)	Matrix 914 (isotropic)	Composite T300/914	Imperfection
$E_f = 230$ GPa	$E_m = 4500$ MPa	$E = 139{,}800$ MPa	$\lambda_0 = 200\ \pi$ μm
$r_f = 3.5$ μm	$G_m = 1600$ MPa	$G = 3817$ MPa	$V_{01} = 1$ μm
$f = 0.6$	$\nu_m = 0.4$		$V_{02} = 0$
			$\phi_0 = 1°$
	Strain hardening (isotropic)		
	$n = 3$	$n = 4.5$	
	$\varepsilon_y^m = 2\%$	$\gamma_y^c = 2.4\%$	

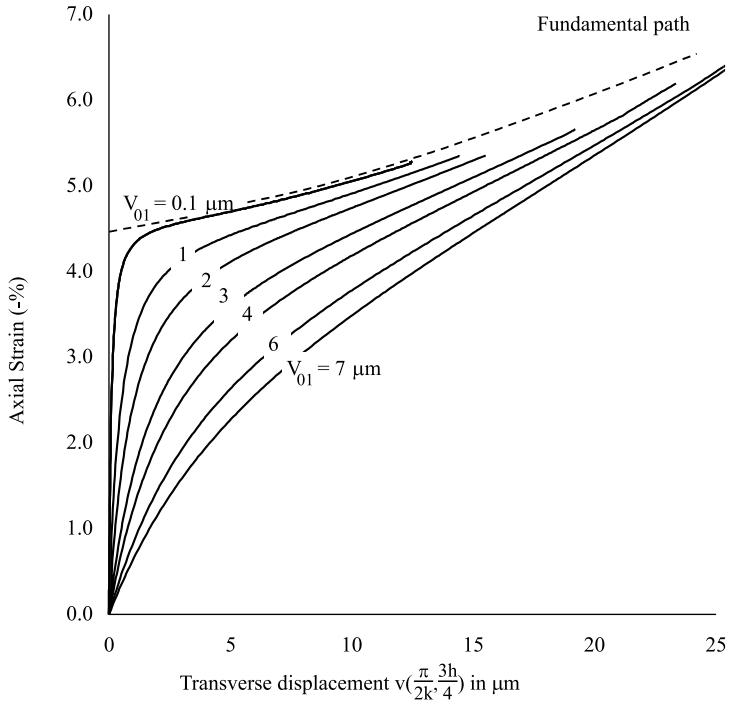

Fig. 2. Elastic response of a UD 1.6 mm thick ply under compression loading.

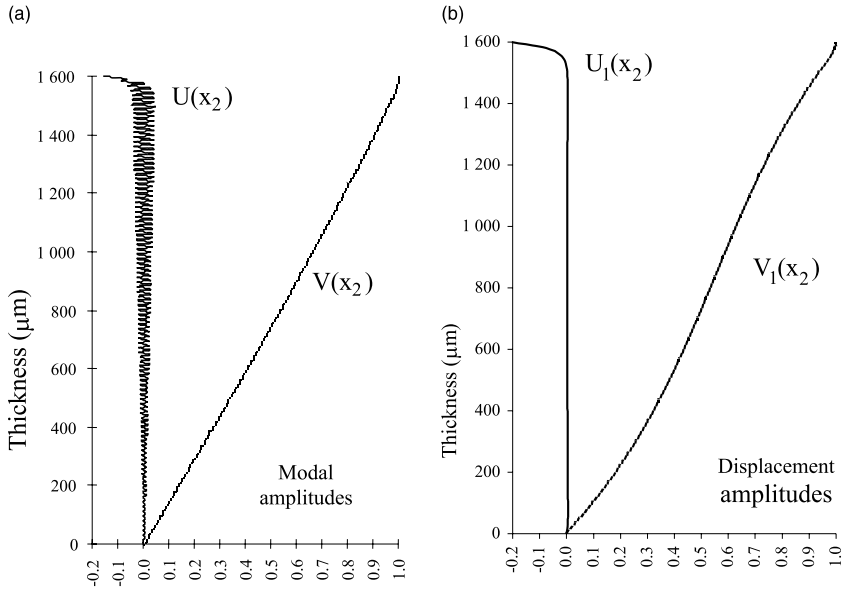

Fig. 3. Displacements for a UD under compression loading; thickness, 1.6 mm, bottom face clamped, top face free (a) modes from the complete discretisation (Drapier et al., 1996), (b) displacements from the present homogenised model $-V_{01} = 0.01$ μm.

to represent later the plasticity development across the thickness and more precisely in the boundary layer. This precaution is essential since it was demonstrated by Drapier et al. (1997) that the plasticity distribution is influenced by the presence of a free edge. For larger imperfection amplitudes, the solution deviates from the fundamental path and the ply stiffness drops drastically for amplitudes greater than 1 μm. Several thicknesses and boundary conditions prescribed on both faces have been investigated and it is found that systematically both the elastic modes and critical loads established by Drapier et al. (1996) can be determined.

In short, our approach permits to characterise properly the elastic microbuckling modes at the ply scale and emphasizes the influence of the imperfection on the elastic response of the ply. These results confirm the validity of the homogenised model proposed here and validates the splitting of the displacement field used to solve the problem at the ply scale.

3. Influence of the material mechanical characteristics

In the present part, the plastic microbuckling mechanism is thoroughly investigated. First, the mechanism is described in detail for a set of given mechanical and geometrical parameters. Afterwards, the influence of the imperfection parameters, i.e. amplitude, shape and distribution across the thickness, are presented and compared with some results obtained through the kink-band model proposed by Budiansky and Fleck (1993). Then, the role of the matrix and fibre mechanical characteristics is described and compared with the trends given by the kink-band model. On the basis of the results from Drapier et al. (1997, 1999), a very thick UD ply (5 mm) is studied whose top and bottom faces are clamped. With this geometry, the effects of the ply structure and boundary layer developing close to any free-edge are prevented. Moreover, a compression loading is considered to avoid any gradient effect induced by the loading. The material studied is of T300/914 carbon–epoxy type, whose matrix behaviour is modelled through a Ramberg–Osgood's type law. The characteristics taken by default are reported in Table 1 and the 914 resin stress–strain curve is plotted in Fig. 4.

3.1. The plastic microbuckling mechanism

In order to focus on the basic mechanism only, a UD ply is studied in which the imperfection wavelength is equal to 0.63 mm and has a constant amplitude across the thickness. The amplitude component V_{01}

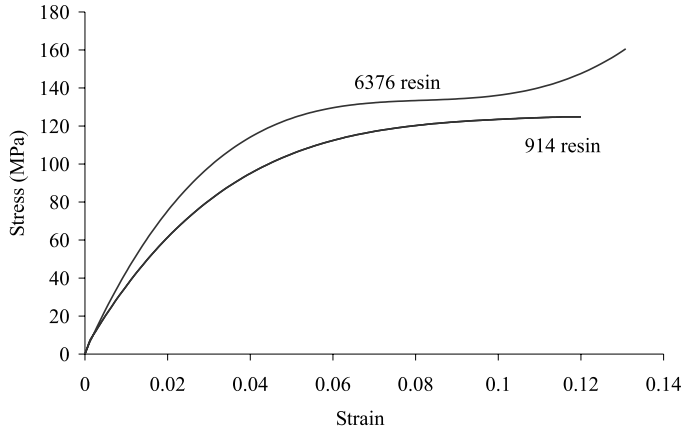

Fig. 4. Stress–strain curves used for resins 914 and resin 6376.

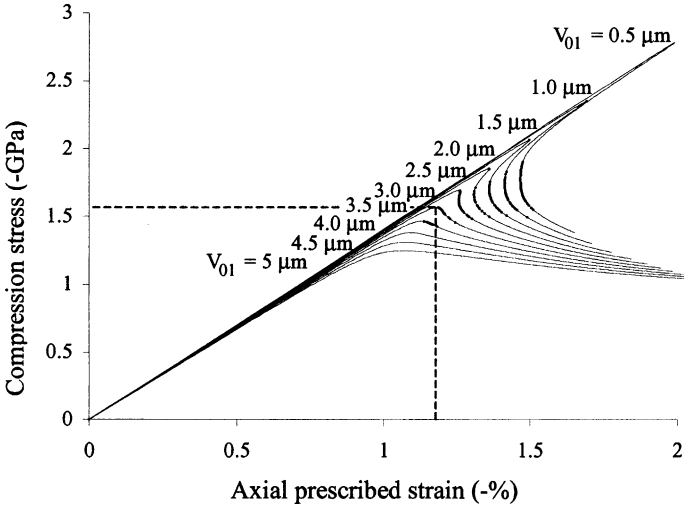

Fig. 5. Plastic response for a UD ply. The imperfection magnitude V_{01} ranges from 0.5 to 5 μm.

ranges from 0.5 to 5 μm, whereas V_{02} is zero. The observations reported in this particular configuration apply equally to the whole set of simulations that follows.

Responses under compression are plotted in Fig. 5 and are identical to the ones obtained by Kyriakides et al. (1995) who performed some finite element computations on a fully discretised region of a UD ply. One can clearly distinguish the stable and unstable responses towards the prescribed strain. Indeed, whereas the solution always exhibits a limit point in load, the limit point in strain is visible only for imperfection amplitudes lower than 3 μm. This value holds only for the present example.

It is assumed that experimentally, the occurrence of the plastic instability leads to the composite failure, since after the limit point neither a load control nor a displacement control can permit to drive the behaviour at the ply scale. By extension, the maximum stress point will be associated with the composite failure and then will be used to define both stress and strain at failure. It must be pointed out that in composites based on high stiffness fibres (GY70 for instance), the fibre failure might trigger the instability occurrence. In the present approach, the fibre fracture is not accounted for due to two main reasons. First, no evidence of such fracture appeared when taking this phenomenon into account in the present model, and second, one faces a lack of data relative to the fibre strength especially in compression.

After Tvergaard (1980), the type of behaviour reported in Fig. 5 is representative of structures that after the limit point exhibit a development of the localisation of plastic deformations. As stated previously, our model cannot represent this localisation, since the solution is sought in a restricted space defined by the displacement field approximation (9). But up to the instability, i.e. at failure, the present model is able to predict quantitatively the ply behaviour.

For fixed mechanical characteristics, the different behaviours for small or large imperfection amplitudes lie mainly on the stress ratios and distributions that lead the unreinforced material in its plastic state. In the next paragraphs are detailed the stress distributions in the mid-ply for both 1 and 4 μm imperfection amplitudes. Only the central part of the ply is studied for plastic microbuckling spreads all over this region. In Figs. 6–9, both developments and distributions are plotted versus both loading and locations along the fibre direction, for the two imperfection amplitudes considered. In those plots, σ_{11} is the HEM longitudinal stress, σ_{12}, the HEM shear stress, σ_{22}, the HEM transverse stress, σ_{Mises}, the von-Mises stress in the matrix and σ_{Bend}, the pure bending stress in the fibre.

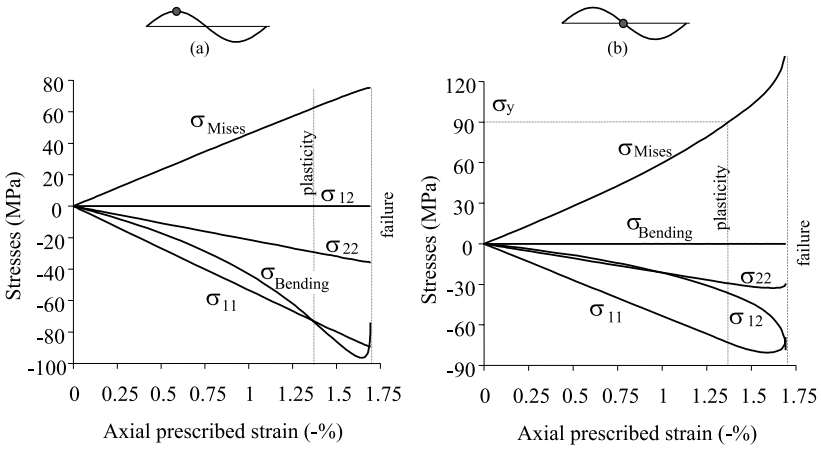

Fig. 6. Stresses versus loading up to the limit point at (a) the point of largest curvature and (b) the point of largest slope. The imperfection magnitude v_{01} is 1 μm.

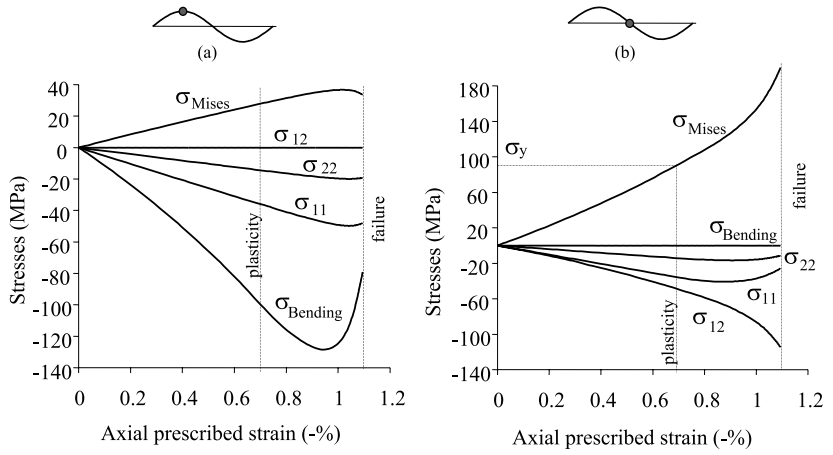

Fig. 7. Stresses versus loading up to the limit point at (a) the point of largest curvature and (b) the point of largest slope. The imperfection magnitude v_{01} is 4 μm.

3.1.1. Failure induced by the ply instability

In Fig. 6 (a) and (b), it can be seen that for small imperfections the fibre bending yields very little matrix shear at the beginning of loading. The direct compressive stress induced by the loading is predominant and leads the matrix in its plastic state for a prescribed strain of −1.37%. Indeed, over a large region of the studied zone, the plastic limit (σ_y, ε_y) is exceeded for the von-Mises stress and nearly reached for the direct compression stress. After this limit the resin stiffness drops quickly which induces a continuous increase of the bending stress at the largest curvature point (Fig. 6(a)). Meanwhile, the shear stress becomes more and more preponderant at the largest slope point (Fig. 6(b)). Just before the instability occurs, a sudden unloading takes place in the fibres (Fig. 6(a)). It is due to the geometrical instability that appears suddenly, inducing a very sharp response of the ply that is mainly controlled by the axial stiffness. This result confirms clearly that it is actually the connection between the fibre bending and the matrix non-linear shear response that originates the instability. After the limit point, the longitudinal compression stress slightly drops at the

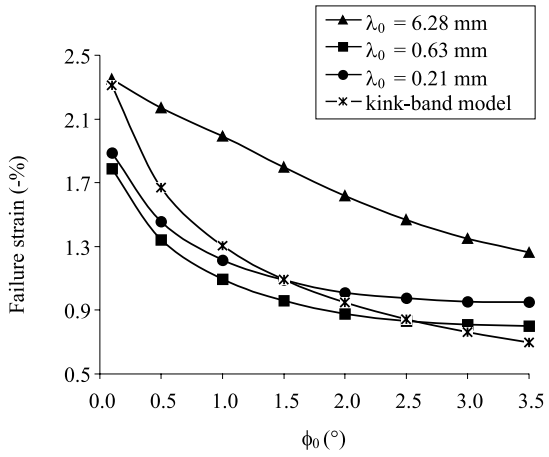

Fig. 8. Strain at failure versus the imperfection angle ϕ_0 for several wavelengths λ_0.

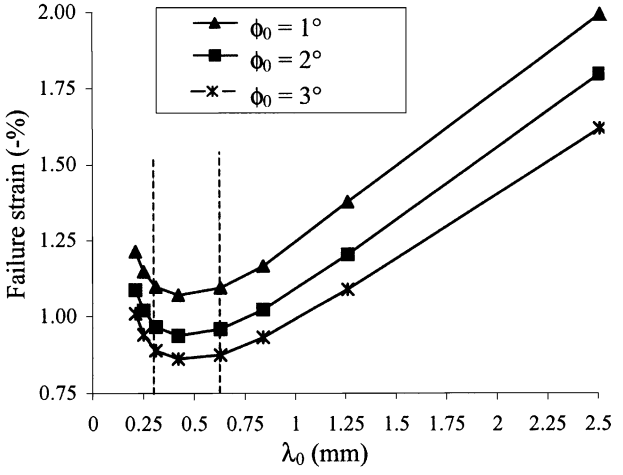

Fig. 9. Strain at failure versus the wavelength λ_0 for several imperfection angles ϕ_0.

largest slope point and the von-Mises stress is continuously increasing all over the domain. This increase is explained by the initiation of plastic shear strain localisation that takes place out of the longitudinal and transverse strains. The maximum load point corresponds to a change in the plastic flow path, which justifies the use of J2 deformation theory type that is efficient enough in characterising such plastic instabilities (Hutchinson, 1974).

3.1.2. Failure induced by a limit load

For a large initial imperfection, the fibre bending (Fig. 7(a))–matrix shear (Fig. 7(b)) connection is the basis of the microbuckling development. Compared to the small imperfection case, the resin is less compressed but it is more heavily loaded in shear as can be seen when observing Figs. 6 and 7. The yield stress is reached in particular locations of the domain for an applied strain of -0.69%. More precisely, the plastic strains localize at the point of maximum slope (Fig. 7(b)). At the beginning of loading, there is a gradual increase of the transverse displacement induced by the growth of fibre bending (Fig. 7(a)) up to the

maximum load. This bending induces high shear strains in the resin (Fig. 7(b)) that give rise to the development of plastic zones, where the mechanical properties quickly drop. This weakening of the matrix induces a larger displacement of the fibres, similar to the occurrence of a geometrical instability of low amplitude. With a 4 μm imperfection, the instability occurs very gradually, since the yield stress is exceeded only at the largest slope points, mainly driven by shear.

After the limit point, the fibre deflection increases gradually and the initiation of plastic strain localization comes along with locally a progressive decrease in the fibre bending stresses. The von-Mises stress is also subjected to a very slight decrease, but only where the plastic limit is not exceeded. Therefore, our hypothesis of no unloading, that justifies the use of a non-linear elastic law to simulate a plastic behaviour, is perfectly well founded.

3.1.3. Synthesis

The mechanism of plastic microbuckling depends essentially on the ratio of the fibre bending stiffness and its elasto-plastic support. Two regimes can be distinguished depending on the initial imperfection amplitude. When the imperfection is low, the matrix plasticity spreads homogeneously all over the domain under the action of the compression stress. This induces the sudden occurrence of the instability. For large imperfections, plasticity develops heterogeneously from the beginning of loading due to the shear induced by the increase of the initial waviness. Then, the fibre deflection increases gradually and a limit point in load is reached. It can be noticed that for large imperfections, it is the yield stress in compression that controls the plastic flow, whereas for small imperfections it is the yield stress in shear.

3.2. Influence of the initial imperfection

3.2.1. Influence of the imperfection wavelength

Previously, it has been demonstrated that the point of maximum slope corresponds to the region with the more pronounced plastic flow. This result on its own justifies why numerous authors assumed that the key parameter in the microbuckling mechanism is the angle made by the fibres with respect to the loading direction. In order to assess this assumption, the effect of both the amplitude, ϕ_0, and wavelength, λ_0, of the imperfection are investigated.

In Fig. 8, failure strains are reported versus the imperfection angle for three different wavelengths. In this figure are also reported the predictions calculated through relation (1) proposed by Budiansky and Fleck (1993) with identical mechanical properties. One can notice that for increasing imperfections, the failure strain decreases whatever be the wavelength predicted by Argon (1972) and Budiansky (1983) and as calculated from relation (1). However, our calculations show that the failure strain is also influenced by the imperfection wavelength. More precisely, it appears a 'critical' wavelength ($\approx$0.5 mm) for which failure strains are the lowest (dotted lines in Fig. 9). In a range around this 'critical' value (0.3–0.6 mm), the failure strain in first approximation depends only on the angle of imperfection, which defines a domain where the kink-band models are valid. But for large (>3 mm) or small (<0.2 mm) wavelengths, failure strains increase significantly, especially for large wavelength imperfections. Consequently, out of the 'critical' range, both parameters (angle and wavelength) must be considered to be of equal importance in defining the imperfection. In the numerous computations carried out on this 'test' ply, the transition between failures characterised by limit points and limit loads always occurs for an imperfection angle of 1.75°, whatever be the wavelength considered.

As shown in Fig. 8, the failure strains calculated from our model are comparable to the predictions from the kink-band model. Let us notice that for fixed wavelengths, the effect of the imperfection angle is not as much pronounced in our model as in Budiansky and Fleck's model (1993). But on the other hand, the 'critical' range of wavelengths (0.3–0.6 mm) lies above the measurements made by Paluch (1994) in a T300/914 material. The wavelengths measured in that study vary from 0.6 to 1.16 mm. Therefore, in order to

yield proper predictions of failure one must take into account both angle and wavelength of the imperfection.

3.2.2. Influence of the imperfection shape

Previous results showed that both wavelength and magnitude of the imperfection affect the microbuckling development. Mainly, these characteristics affect the stress field distribution in the matrix and thus the distribution of matrix plasticity. One can, therefore, expect the distribution of imperfection across the thickness to affect the microbuckling mechanism too. However, at the moment, very little is known about the imperfection distribution in composites. Hardly a couple of studies have been devoted to the measurements of imperfection amplitudes and wavelengths of few tens of fibres. Paluch (1994) has shown that the imperfections do not have a perfect configuration in the fibre direction. However, one can attempt to evaluate the effect of the spatial distribution of the imperfection on the compressive strength of UD plies.

Fibre waviness is first modelled with a single harmonic (wave number k). All the fibres are affected by the same imperfection which can vary in three manners across the thickness. First, the distribution is constant, second, the distribution follows the elastic mode shape and third, the distribution is opposite to that mode. The structure studied is a UD ply, 1.6 mm thick, with two sets of boundary conditions that represent the position of this ply in a laminate stacking sequence. First, both top and bottom faces are clamped and second, only the bottom face is clamped. The imperfection angle is 1° or 2.5° and its wave length is 0.63 mm. These choices must permit to split up in the development of plastic microbuckling, the contribution of the initial imperfection distribution (and therefore, the matrix plastic flow heterogeneity) from the contribution of the elastic buckling mode (purely geometrical non-linearity).

In Fig. 10 are reported the failure strains for both sets of boundary conditions and both imperfection angles. It is clear that the lowest strength is obtained from the constant distribution across the thickness which yields the largest zone affected by the highest matrix plastic flow. This result confirms that the role of the imperfection distribution is essential in setting the spatial distribution of the zones wherein plasticity develops. Comparison of the strains at failure calculated with modal and anti-modal distributions show that the plastic microbuckling development results from a combined effect of the distribution of geometrical instability and material non-linearity, as suggested by Drapier et al. (1997). These remarks hold for both sets of boundary conditions and imperfection angles. This suggests that it is a systematic character of these results.

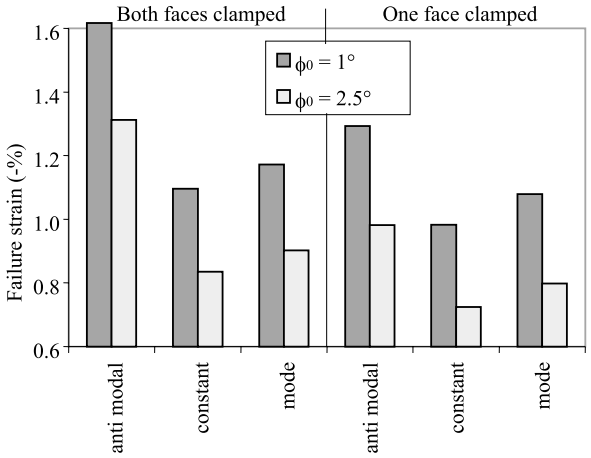

Fig. 10. Effect on the failure strain of the imperfection distribution across the thickness.

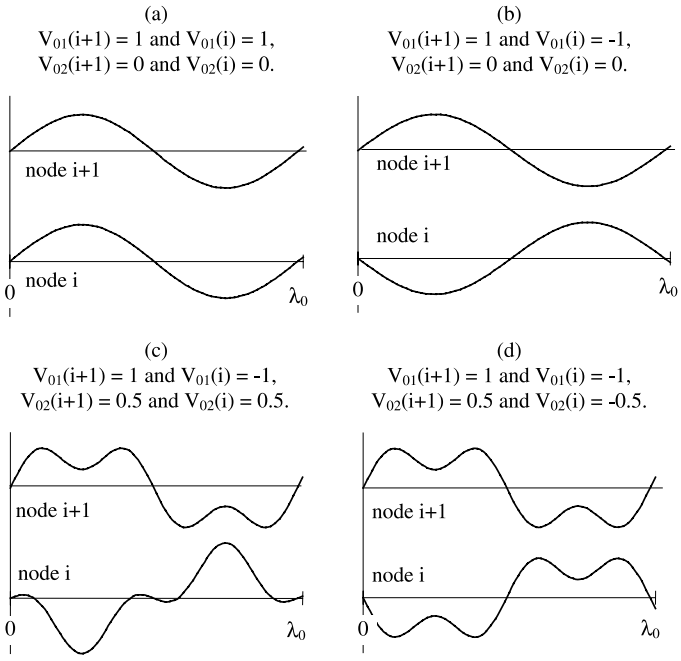

Fig. 11. Shape of the imperfection built with several amplitudes V_{01} and V_{02} (μm).

In this second part, four distributions along the fibre direction are chosen and are plotted in Fig. 11, where they are referred to as (a)–(d). The complete description of the imperfection over the domain is obtained by repeating periodically each of the four patterns in transverse and axial directions. The structure studied is a 1.6 mm thick ply whose faces are clamped and the imperfection wave number is here $k = 0.01$. Whatever be the distribution considered, the ply response remains identical, only the strains at failure vary significantly. The lowest failure strains are obtained with imperfections (a) and (c) (1.69% and 1.63%, respectively). Let us notice that the in-phase imperfection (a) does not yield the smallest failure strain as could be expected. Conversely, the phase-opposition imperfection (b) yields the highest strength (2.14%) and (d) distribution leads to an intermediate value of 1.93%. In these results appear again the major role of the bending-induced shear on the instability development. Indeed, configurations (a) and (c) that correspond to the lowest strength induce high matrix shear that facilitates the plastic flow. The other distributions induce a more complex strain state in the matrix that delays the plasticity development. The discrepancy on failure strains between configurations (a) and (c) is far from negligible (0.51%). We think that the large difference between the in-phase and phase-opposition distributions is mainly due to the contribution of the elastic mode, i.e. the geometrical non-linearity on its own (Drapier et al., 1997).

These results confirm the central role played by the imperfection. Thanks to the various capabilities of the present model, we establish not only the effect of the imperfection angle and imperfection wavelength but also the spatial distribution of this imperfection (both across the thickness and in the fibre direction). As far as the authors know, these are new results.

3.3. Influence of the constituents mechanical characteristics

As numerous authors pointed out, the microbuckling mechanism is strongly influenced by the matrix plastic behaviour. For instance, in the kink-band model considered here for comparison, an analytical

expression of the failure stress (1) was proposed as a function of the composite yield stress and the composite shear strain hardening. Predictions from this model are in good agreement with some experimental results and in the present paragraph, they are compared with the ones obtained from the present numerical tool.

In order to minimise the effects of the structural parameters, the various computations are carried out on a 5 mm thick UD ply, whose both faces are clamped. The influence of each material parameter is studied independently from the others.

3.3.1. Matrix

In Budiansky and Fleck (1993), the composite behaviour is modelled through a law of Ramberg–Osgood's type. The composite shear strain γ is related to the composite shear stress τ by the following constitutive law (11):

$$\gamma = \frac{\tau}{G}\left(1 + \frac{3}{7}\left(\frac{\tau}{G\gamma_y^c}\right)^{n-1}\right), \tag{11}$$

where G is the composite elastic shear modulus, n is the strain hardening coefficient and γ_y^c is comparable to a yield strain in perfect plasticity for the composite. With the form of the non-linear law (11), the authors proposed an analytical expression of the stress at failure. But with this expression, the response non-linearity is a complex function of both parameters n and γ_y^c. Indeed, this can be seen in Fig. 12(a), where the shear stress is plotted versus the shear strain for various values of n. It can be noticed that below the limit γ_y^c, the loss of stiffness is less important for large n, whereas above γ_y^c, the stiffness change versus n is inverted. In order to avoid this drawback, a law with a threshold is chosen (Fig. 12(b)) for the unreinforced material. Then, in our approach, the drop in stiffness depends only on a strain hardening coefficient, denoted by m, and it takes place when the equivalent strain exceeds the matrix yield strain ε_y^m. This particular choice (Fig. 12(b)) permits to evaluate separately the influence of each parameter (yield strain, elastic stiffness, strain hardening change, etc.).

It is important to notice that a couple in the present approach (m, ε_y^m) corresponds to a couple in the kink-band model (n, γ_y^c). In the results presented in the next paragraph, parameters (n, γ_y^c) are chosen such that the matrix constitutive law in shear is similar for both models of the plastic behaviour. In such a framework, the predictions yielded by the kink-band model and by our model can be compared quantitatively. Since in our numerical tool, the development of microbuckling is tackled through an incremental scheme driven by the prescribed macroscopical strain, the latter is used to compare our results to those

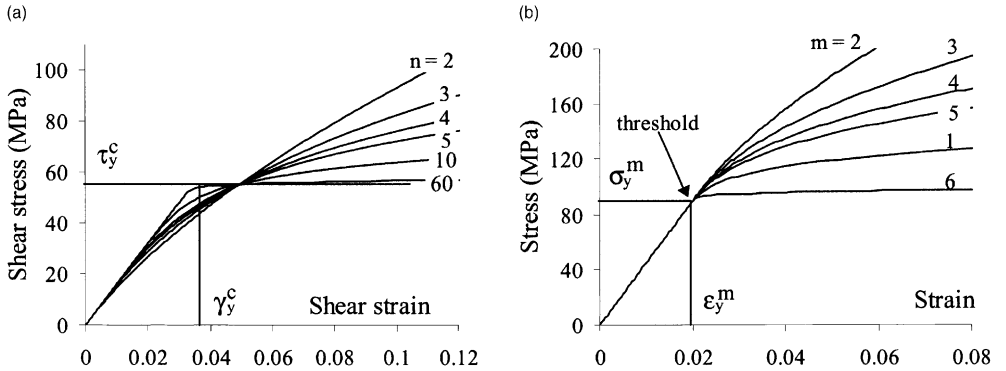

Fig. 12. Constitutive laws used: (a) in Budiansky and Fleck (1993) and (b) in the present approach.

from the kink-band model. From the expression of the failure stress (1) the (macroscopical) failure strain is easily derived with the following relationship:

$$\varepsilon_c = \frac{G}{E}\left(\frac{1}{1+n\left(\frac{3}{7}\right)^{1/n}\left(\frac{\bar{\phi}/\gamma_y^c}{n-1}\right)^{(n-1)/n}}\right), \tag{12}$$

where E is the composite Young's modulus.

3.3.1.1. Strain hardening coefficient. First, the matrix yield strain ε_y^m is set to 2%, and elastic (initial) stiffnesses of both constituents are fixed, whereas the matrix strain hardening coefficient (m) varies from 2 to 20. Two imperfection angles of 1° and 2.5° are considered, their distribution is constant across the thickness and their wavelength is 0.2 mm.

In Fig. 13, are reported failure strains calculated from both models. It can be noticed that our predictions are always larger than the ones from kink-band model. This discrepancy is natural since when the fibre bending stiffness is accounted for in the process of kink band formation, predictions (1) and (12) must be raised from 5 to 10% as stated in Fleck et al. (1995a). This is justified by the results presented here and in Section 3. For both imperfection amplitudes, the contribution of the fibre bending in the microbuckling process is essential (Figs. 6 and 7), but more markedly for large imperfections. This latter effect is not taken into account in the kink-band theories and justifies the discrepancies observed in Fig. 13.

Second, for strain hardening coefficients larger than 8, failure strains hardly vary and are quite close for both models. They tend towards a finite value that corresponds to the composite strength, whose matrix would be ruled by a perfectly plastic law. Conversely, for strain hardening coefficients lower than 8 predictions from both models diverge. The maximum discrepancy between predictions from both models is observed for a large imperfection and small strain hardening coefficients. It seems that plies affected by a 2.5° imperfection angle are slightly more sensitive to the changes in the non-linear response of the matrix. As has been demonstrated previously, for large imperfections, the instability is induced by the drop in shear mechanical characteristics and therefore, the behaviour depends strongly on the matrix response. Whereas for small imperfections, the instability arises from the coupling of the stiffness drop with the geometrical non-linearity induced by fibre bending. Thus, changes in the matrix response are not fully passed on to the composite behaviour for small imperfections.

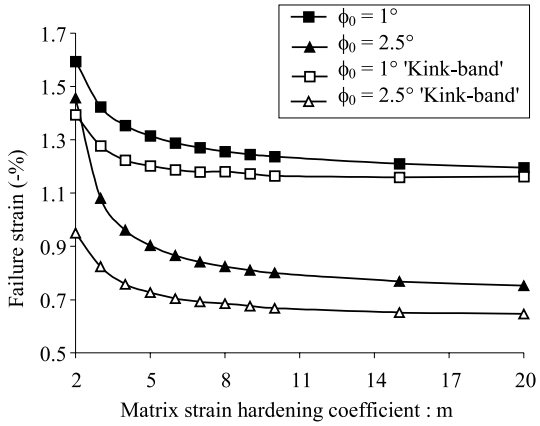

Fig. 13. Failure strain versus the strain hardening coefficient of the matrix m.

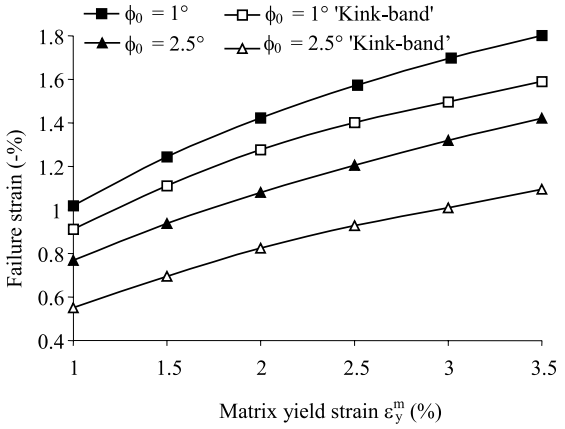

Fig. 14. Failure strain versus the matrix yield strain ε_y^m.

It is important to point out that the influence of the strain hardening coefficient presented here is a new result. Indeed, when relation (12) is used with several strain hardening coefficients n (Fig. 13), only a very feeble difference can be observed (Budiansky and Fleck, 1993). This is based on the expression of the constitutive law whose elastic threshold depends on the combination of both strain hardening and yield strain, as explained previously in this section.

3.3.1.2. Yield strain. These results demonstrate that the central role of the elastic threshold proposed by many authors is to be reconsidered. To validate this, the influence of the yield strain on the strength is quantified (Fig. 14). The matrix strain hardening coefficient is set to 3. Comparing the changes in strength when the yield strain varies (Fig. 14) with those presented previously (Fig. 13), one can notice that both effects are of the same order of magnitude. When the yield strain increases, the stress necessary to increase the plastic flow also increases. It results in an improvement of the ply strength whatever be the imperfection angle. If failure strains predicted by our model are larger than those from the kink-band model, the changes are similar.

Previous results demonstrate the central role of the change in tangential stiffness. This idea is reinforced by the curves plotted in Fig. 15, where an improvement of the strength can be seen when the matrix elastic stiffness increases. In that case, the tangential stiffness drop is delayed as a direct consequence of the yield stress increase since both yield strain and strain hardening coefficients are fixed to 2% and 3, respectively. Failure strain changes that are predicted here are similar to the ones from the kink-band model for both imperfection angles considered. Again, the discrepancy between the predictions from both models (Figs. 14 and 15) can be attributed to the fibre bending stiffness since the largest difference is systematically observed for large imperfections.

To summarise, the relative variation of failure strains versus the various parameters demonstrates that the matrix plays actually a central role. But unlike the statements made by several authors, it appears that the instability is mainly influenced by the change in the tangential stiffness. This latter effect is a direct function of the matrix mechanical characteristics, but depends also on the tridimensional stress state when plasticity occurs which differs for small and large imperfections.

3.3.2. Fibres

The intrinsic fibre characteristics come into play twice in the compressive failure. As seen previously, the fibre bending has a destabilising effect and hence participates in the failure mechanism. But it has to be

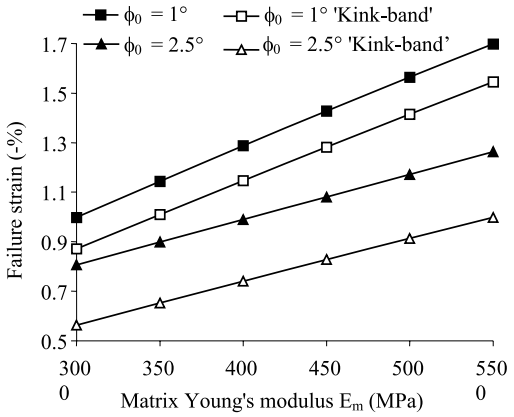

Fig. 15. Failure strain versus the matrix Young's modulus E_m.

noticed that the ply response before the instability strongly depends on the fibre modulus. Three fibre stiffnesses are considered here (230, 290 and 350 GPa) and the 5 mm thick ply response is established for two imperfections (1° and 2.5°). Observation of stresses and strains taken at the failure of the ply show that the ratio of fibre bending to matrix plasticity is fairly constant. Also, it can be noticed that the fibre bending stresses at the limit point are constant for the three moduli considered. It results in a very low dependence (variation lower than 4%) of the failure stresses to the fibre Young's modulus (Fig. 16). Conversely, since the ply elastic stiffness is based on the fibre elastic stiffness, the failure strain strongly decreases for increasing fibre moduli. This clearly appears in Fig. 16 where it can also be seen that predictions from the kink-band model lead to similar changes in failure strains for both imperfections considered.

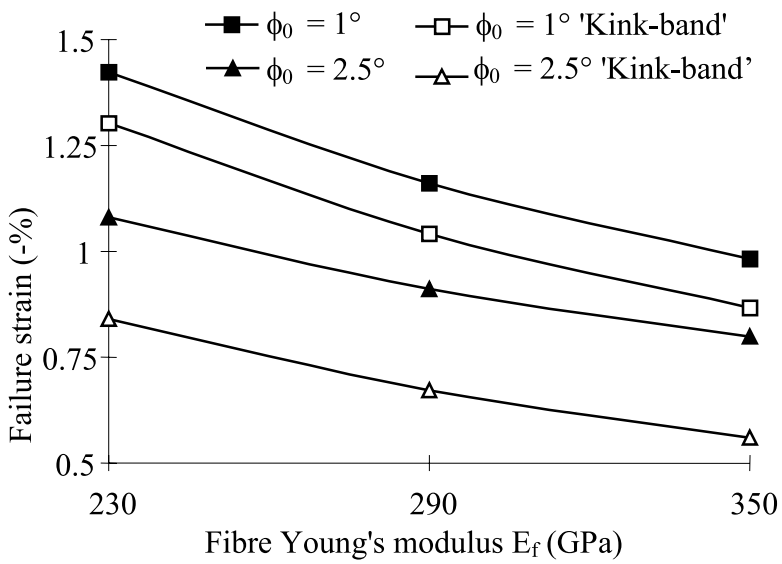

Fig. 16. Failure strain versus the fibre Young's modulus E_f.

3.4. Synthesis

The mechanism of compressive failure is characterised by two different regimes depending on whether the imperfection is small or large. But in both cases the equilibrium between the fibre bending and the matrix stiffness is the basis of plastic microbuckling occurrence. The difference is due to the way in which the matrix reaches its plastic state. For small imperfections, it is mainly the compression stress that originates plasticity whereas for larger imperfections, it is the shear induced by the fibre waviness increase that initiates it.

The fibre initial imperfection is a key element of the plastic microbuckling mechanism. It can be characterised by the maximum angle measured between the fibre and its theoretical (straight) axis, i.e. the point, where the localisation of plastic strains develops, which leads to the ply failure. However, this simplification of the imperfection is valid only in a range of wavelengths for which failure strains are minimum and remain almost constant for the given imperfection angles. For small and large wavelengths, such as the ones measured experimentally, both parameters (angle and wavelength) are necessary to represent the effect of the imperfection on the plastic microbuckling mechanism.

The influence of the mechanical characteristics that we predict is in perfect accordance with the literature. Choosing a threshold function permits to split up the role of the strain hardening from the role of the yield strain (stress). It appears that the change in tangential stiffness is the main parameter that affects the instability mechanism. If the fibre bending influences the failure stress little, it is opposite for the failure strain that increases largely for increasing fibre moduli.

4. Influence of the structural parameters and comparison with experimental results

In the work by Drapier et al. (1999), the influence of the loading, ply thickness and boundary conditions prescribed on bottom and top faces have been extensively described. A complementary part is developed here, where the microbuckling is studied in a complete laminate. The whole thickness of the composite is discretised and free faces conditions are prescribed on both faces. Characteristics of the fibre initial imperfection are very rare and therefore a range of imperfection angles is considered. The other characteristics of the imperfection are not very well known either, or not known at all. Consequently, first, several imperfection angles are considered to grasp at the best the actual compressive strength of the material. Second, because no experimental information can be found that describe the imperfection distribution across the ply thickness, a parabolic distribution is chosen with the largest waviness amplitude located at mid-height.

As has been demonstrated that the imperfection plays a great role in triggering microbuckling, the distribution across the thickness is essential in predicting structural plastic microbuckling development. Then, the imperfection distribution that is chosen is driven by the understanding gained in the field of the imperfection birth and growth (Jochum et al., 1999). More precisely, fibre waviness seems to result from the occurrence of fibre microbuckling induced by the resin shrinkage during the reticulation stage. If this chemical reaction is exothermal and thermo-stimulated, then the shrinkage is larger for fast reactions. This is confirmed by experiments carried out on single-fibre specimens. Consequently, a relationship does exist between the resin shrinkage, fibre initial waviness, and temperature distribution across the ply thickness during cure. Studying thermal exchanges during the curing process shows first that temperature is maximum at mid-thickness and second that the distribution is parabolic in first approximation. Hence one can postulate that the resulting fibre imperfection will be parabolic with the largest amplitude at mid-thickness. This distribution will be used throughout the present section.

In the present framework, the influence of the loading, thickness and stacking sequence on the compressive strength is studied. Since the whole ply is discretised, no hypothesis on the interaction between plies

Table 2
Data for T400 fibres and 6376 resin

Fibre T400 (isotropic)	Matrix 6376 (isotropic)
$E_f = 250$ GPa	$E_m = 4.5$ GPa
$r_f = 3.5$ μm	$G_m = 2.91$ GPa
$f = 0.6$	$\nu_m = 0.33$
	Strain hardening (isotropic)
	$n = 6.5$
	$\varepsilon_y^m = 1.8\%$

is necessary unlike in Drapier et al. (1999). Moreover, the constitutive laws used are based on realistic characteristics of the components such that comparisons can be made between results from our computations and experimental results from the literature. Fibre and resin characteristics are detailed in Tables 1 and 2 and experimental stress–strain curves used for both 914 and 6376 resins are plotted in Fig. 4.

4.1. Loading

Experimental bending tests have demonstrated that a T300/914 composite can locally withstand more than 2% of compression. Conversely, if the same material is tested under pure compression, its strength is about 1.2% (t'Hart et al., 1991). In order to explain this difference, two configurations are investigated here for a 3.2 mm thick UD ply. In the first case, the loading is constant across the thickness (pure compression), whereas in the second case the loading varies linearly through the thickness and vanishes at mid-thickness (pure bending). The imperfection angles range from 0.1° to 2° and the wavelength remains equal to 0.9 mm according to Paluch's measurements (1994) ranging from 0.6 to 1.16 mm.

In Fig. 17 are reported strain at failure for several computations carried out on a T300/914 like material. One can notice that with both loadings the larger the imperfection, the lower the laminate compressive strength. Also, the strength is systematically higher under pure bending loading. With imperfection angles close to 0.5°, our prediction of the compressive strength correlates very well with experimental measurements (t'Hart et al., 1991) for both compression (1.2%) and bending (1.95%). Predictions obtained through

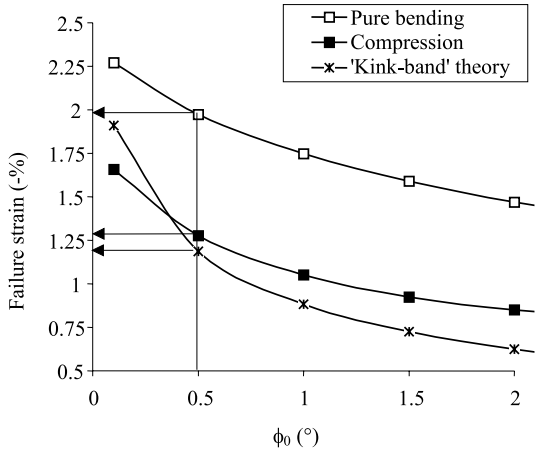

Fig. 17. Failure strain versus the imperfection angle ϕ_0 for compression and pure bending loadings.

the kink-band model are close to the ones obtained under pure compression (Fig. 17), which supports the validity of relation (1) under simple conditions.

The influence of the imperfection angle on the compressive strength is similar for both compression and bending loadings. This result clearly demonstrates that the scattering of results that pure compression devices exhibit (t'Hart et al., 1991) must be essentially attributed to the compression rigs themselves rather than to the fibre misalignment imperfection. Indeed, if fibre initial imperfections can initiate scatterings in measurements, from the simulation, this discrepancy should be observed for the bending devices too, but this is not the case. This conclusion is confirmed by results from the simulation of pure compression devices carried out by Anthoine–Rahier and Grandidier (1996). These authors have shown that testing devices are very sensitive to any manufacturing and positioning imperfection. These imperfections induce tridimensional stress states in the grips that lead to the premature failure of the material in these places.

In Fig. 17, it can also be noticed that the difference in strength obtained from the two loading configurations is rather constant whatever the angular imperfection. This result is justified by the displacement and stress distributions across the ply thickness which are proper to each loading and are independent of the imperfection. Under pure compression loading, both strain and stress distributions are fixed by the imperfection distribution across the thickness. Indeed, matrix plasticity develops in the central zone of the UD ply but does not localize in the boundary layer close to the free face, as could be expected. The maximal von-Mises stress is reached in the centre at the largest slope points (Fig. 18). Conversely, under bending this zone in which plasticity develops is reduced to a third of the ply thickness, and it is situated in the part undergoing compression (Fig. 19). More precisely, a boundary layer appears according to the presence of the free edge. It seems that the loading counterbalances the effect of the imperfection distribution which is no longer predominant in setting the microbuckling distribution. The characteristic transverse length, i.e. the dimension of the zone in which microbuckling will develop and thus control the laminate response, is fixed by the gradient of loading.

To summarise, in the presence of imperfection distributions, under pure compression loading, plastic microbuckling will develop accordingly to the maximal misalignment amplitude. Conversely, under bending loading, the gradient of loading is predominant in setting the plastic microbuckling development. Therefore, the imperfection distribution will play only a minor role regarding the spatial distribution of microbuckling.

4.2. Thickness

In order to evaluate the influence of the thickness on the characteristic transverse dimension, computations have been carried out for UD plies whose thickness ranges from 0.25 to 12.8 mm. Angular imperfections considered are 0.5° and 1.5° with the same wavelength of 0.9 mm. Results from the simulations are compared with measurements from bending experiments achieved by Wisnom (1991) on XAS/913 material. Data for this type of fibre and resin are quite close to the ones from T300/914 material and consequently these latter data will be used for the present comparison.

It can be observed in Fig. 20 that under pure compression the thickness has very little influence on the laminate strength. This result can be justified first by the homogeneous strain and stress distributions, and second because the influence of the boundary layers close to the free faces is limited by their small size. Only for very thin composites, the region in which plasticity develops is of the same size as boundary layers, and this induces a slight decrease in the compressive strength. Therefore, except the influence of the boundary layers for very thin laminates, there is no structural effect under compression since there is no characteristic transverse length prescribed: both faces are free and the loading is constant across the thickness. From there, only a distribution of imperfection across the thickness can induce a structural effect as it was demonstrated in Section 3.2.2.

Conversely, under a bending loading, a decrease in thickness yields an increase in failure strain for both imperfections angles considered. This strength increase is induced by the decrease of the zone undergoing

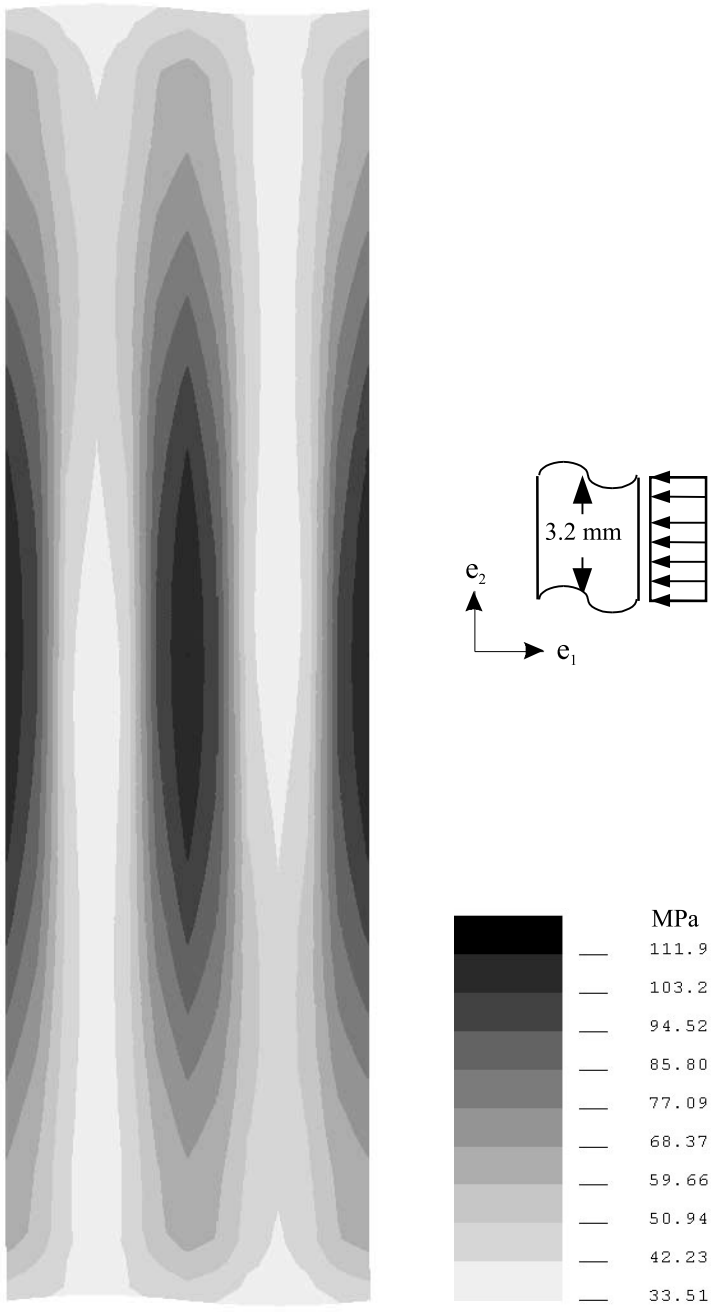

Fig. 18. Von-Mises stress distribution (MPa) in the resin at failure load. Case of compression loading for a 3.2 mm thick ply. Deformed shape × 10.

compression when the thickness decreases. In other words, when the gradient of loading increases beyond 3.2 mm, the influence of the thickness becomes small which confirms the results from Drapier et al. (1999).

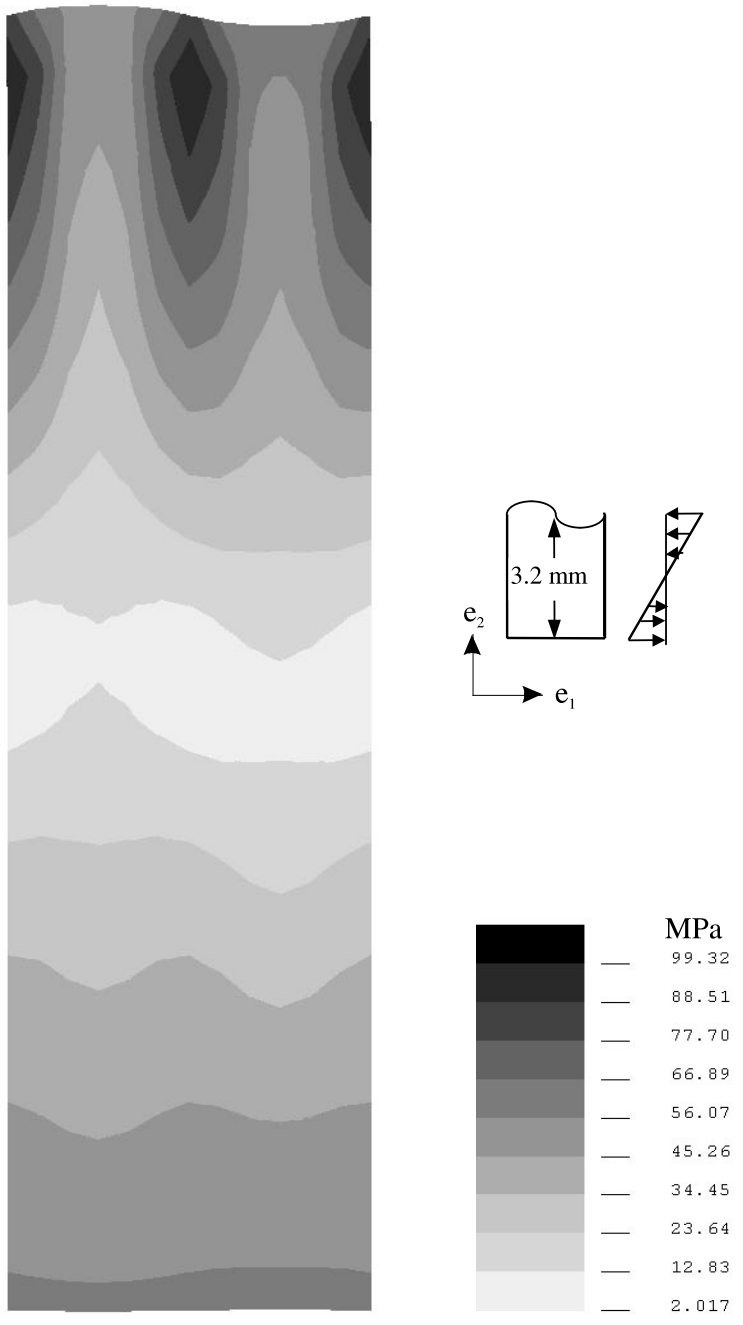

Fig. 19. Von-Mises stress distribution (MPa) in the resin at failure load. Case of pure bending loading for a 3.2 mm thick ply. Deformed shape × 10.

Wisnom (1991) tested UD carbon–epoxy XAS/913 with 60% volume fraction of fibres. Specimens were manufactured with pre-impregnated material 0.125 mm thick and 25, 50 and 100 layers which lead to

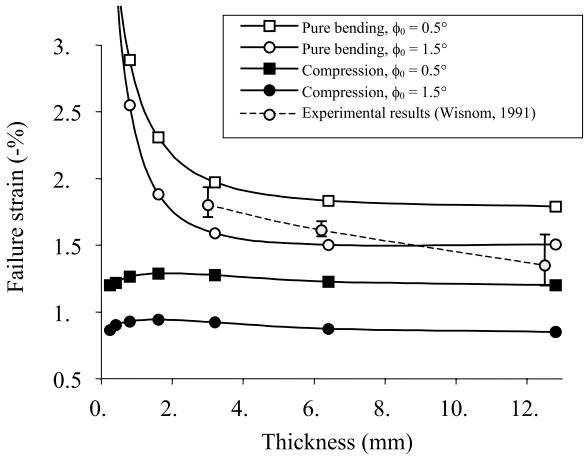

Fig. 20. Failure strain versus the UD thickness.

measured thicknesses of 3.175, 6.35 and 12.38 mm respectively. Failure strains were measured in tension and compression with a pin-ended-buckling test and a four-points bending rig. For this comparison, only failure which occurred on the compressed face were considered. In Fig. 20, it clearly appears that our predictions can correlate the experimental results at least for the two thinner plies for which the gradient is the most pronounced. For thick specimens, a drop in measured strength is observed that is related either to manufacturing defects or to the presence of larger waviness amplitudes as suggested by our computations. Also, as pointed out by the author (Wisnom, 1991), the cure process used for the thicker specimen is different from the process used for the thinner ones. Eventually, it is worthwhile pointing out that the imperfections considered here are restrictive and that further information is required to improve the comparison between theory and experiments. Especially if one realises that fibre initial imperfections are controlled by both geometrical and processing parameters.

4.3. Gradient of loading

It was demonstrated previously that both the loading and thickness of UD plies has a great influence on the compressive strength. The combination of these two parameters results in setting the gradient of loading across the thickness. This confirms the work of Grandidier et al. (1992) who established through a combination of experiments and computations on glass/epoxy material that high gradients of loading yield higher strength. In an elastic framework, a model was proposed which led to qualitative prediction of this phenomenon.

Variation of this parameter can result from the combination of a varying thickness with constant maximum load applied, but also from a bending state that is no longer pure bending. In this part are compared predictions from our model with experimental results of Wisnom et al. (1997) who tested with pin-ended buckling rigs some T800/924 material. In this work, specimens of various dimensions were tested, especially the thickness and length varied which led to gradients of loading across the thickness ranging from 0.325% to 3.83% mm^{-1}.

Characteristics considered here for the computations are similar to those for a T300/914 material (Table 1). In Fig. 21, it can be seen that our predictions correlate well with the experimental results of Wisnom et al. (1997) which in first approximation relates linearly the compressive strength to the gradient of loading. The small discrepancy that exists between predictions and experiments may be related to imperfections that are

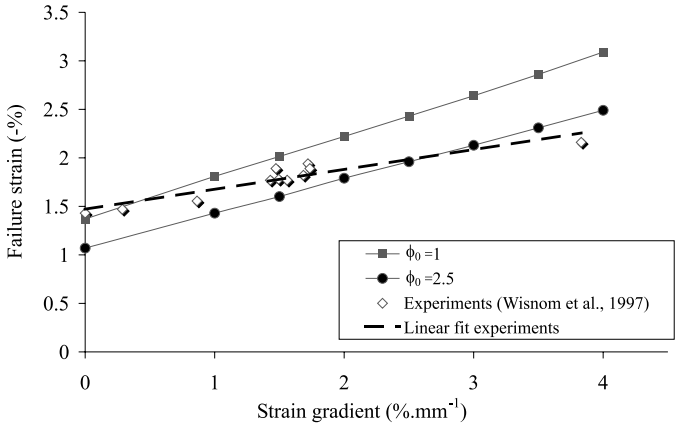

Fig. 21. Failure strains versus the gradient of loading for UD plies, for experimental results (Wisnom et al., 1997) and predictions from the present model.

not in reality as homogeneous as considered in the model. From the effect of the loading and thickness, it is clear that the effect of the gradient of loading is to set the characteristic length upon which microbuckling develops. This role of the gradient of loading is in agreement with the work of Drapier et al. (1996), who studied the elastic microbuckling mode at ply scale, but also with the work of Drapier et al. (1997) who reached the same conclusion on single UD plies.

This comparison demonstrates first, the ability of our model to account for the effect of structural parameters. Second, with reasonable imperfection angles a quantitative prediction of the effect of the gradient of loading is proposed. This effect is the very one that affects the compressive strength, although its influence can appear either through varying thickness or loading. This explains why demonstrating its influence is not straightforward and very sparsely considered in the literature. And as far as the authors know, the effect of the gradient of loading on the compressive strength of composites has never been predicted either qualitatively or quantitatively.

4.4. Stacking sequence

In this part, the influence on the instability of the stacking sequence and of the cross plies (90° and 45°) stiffness is investigated. Six laminates are considered which are made up of 16 plies: $[0_{16}]$, $[0_3,90]_{2S}$, $[0_2,45_2]_{2S}$, $[0_2,90_2]_{2S}$, $[0,90_3]_{2S}$ and $[0,90]_{4S}$. Among these sequences, four families can be distinguished, which are characterised by a similar number of neighbouring 0° plies (16 plies, 3 plies, 2 plies and one ply).

It is evident that whatever the loading considered the thicker the consecutive neighbouring 0° plies, the lower the compressive strength (Fig. 22). The presence of transverse plies at 90° or 45° set the characteristic transverse length by clamping the fibre transverse displacement close to the interface between the 0° ply and the transverse ply. Let us notice that regarding the instability, the support provided by transverse plies is similar since the compressive strength of $[0_2,45_2]_{2S}$ and $[0_2,90_2]_{2S}$ laminates are identical. On the contrary, the transverse plies thickness does play a role, since in $[0,90]_{4S}$ laminate microbuckling develops in both internal and external 0° plies. This yields a slight drop in strength when compared to $[0,90_3]_{2S}$ laminate for which microbuckling occurs in the external plies only.

The difference in strength between compression and bending is maximum for the $[0_{16}]$ stacking. This is due to the fact that the difference in size of the zone where plasticity develops is larger between the two loadings for UD plies. In the case of laminates, the dimension of the plastic zone is essentially influenced by the thickness of the 0° consecutive plies. When this latter becomes small, the loading no more influences the

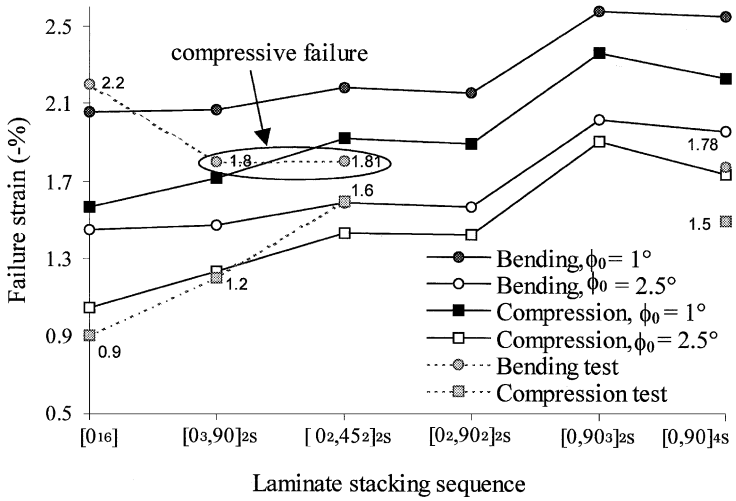

Fig. 22. Theoretical and experimental failure strains versus laminate stacking sequences.

strength. It must be pointed out that contrary to the previous section, there appears a structure effect under compression loading which is induced by the thickness of consecutive 0° plies.

The comparison attempted here with experimental data is partial, since very few works can be found in the literature which deal with this problem. The present approach considered from Grandsire-Vinçon (1993) was carried out on T400/6376 material whose behaviour is represented through the data given in Table 2 and in Fig. 4. Laminates were tested using pure compression and pin-ended buckling experiments. Results from experimental measurements are reported in Fig. 22. It appears that our predictions are in good agreement with the experimental tendencies, but these new results must be validated by a consistent experimental work that is in progress at the moment.

5. Conclusion

In this article, the compressive strength of composite laminates has been investigated, thanks to a specific finite element. The model underlying this numerical tool permits for the first time to capture the development of the plastic microbuckling mechanism in laminates while taking into account the effect of structural parameters.

In terms of response, systematically two characteristic responses of the ply can be observed. For small fibre imperfections, the matrix plasticity appears homogeneously in the material under the action of the compressive stress. This leads quickly to the sudden occurrence of the geometrical instability characterised by a limit point both in loading and displacement. For larger imperfections, plasticity appears heterogeneously from the start of the loading under the action of shear induced by the initial waviness. Then, fibre waviness increases progressively and a limit point in load is reached.

Those results confirm that the fibre initial wavy imperfection is one of the key parameters for failure induced by plastic microbuckling. It can be characterised by the maximum angle that exists between the fibre and its theoretical direction (loading direction). However, as it has been demonstrated, this simplification of the imperfection holds only for a narrow range of wavelengths, for which failure strains are minimum and depend only on the angle. This range of wavelengths has proved to differ from measurements of imperfections made on actual composites. Then, both parameters (wavelength and amplitude) are necessary in order to get realistic predictions of the compressive strength limited by the plastic micro-

buckling mechanism. Our approach also permitted us to quantify the influence of the spatial distribution of the imperfection. Simulations led to the conclusion that the lowest failure strains correspond to a constant imperfection across the thickness. But the comparison of failure strains obtained when considering a modal and anti-modal imperfection distribution demonstrates that the elastic (geometrical) mode participates too in the development of plastic microbuckling. The form of the imperfection in the loading direction influences significantly the strength. This is a result that calls for a better understanding of the fibre initial imperfection.

A parametric study was carried out on the constituent mechanical characteristics which validates our model and completes the results from kink-band theories. Clearly, the combination of fibre imperfection with matrix plasticity is a central element of failure induced by plastic microbuckling. The constitutive law with a threshold that was used for the matrix has permitted to grasp the influence better, of the yield strain (and stress), strain hardening, and elastic stiffness on the compressive strength. The results show that the central role that many authors assign to the threshold must be reconsidered since a tangent stiffness criterion seems more appropriate in predicting the compressive failure. Comparison with the kink-band theory demonstrates that our approach, which does not aim at describing in deep details the plastic microbuckling mechanism, permits to tackle very properly this instability.

Then, our structural model, including also the effect of the local parameters, was used to demonstrate and explain the effect of both thickness and loading. Computations carried out on UDs provided a rigorous explanation of the high strength of composites achieved under bending loading. Combination of the loading along with the laminate thickness results in setting the dimension of the zone in which microbuckling develops and consequently sets the strength of the whole ply. More precisely, for a UD ply under bending loading, the thinner the ply the larger its strength. Beyond 3 mm, the effect of the thickness is no longer significant. Under pure compression, no structure effect can be observed on the UD ply since no transverse characteristic length is prescribed. In accordance with some experimental evidences, the compressive strength was shown to depend in first approximation linearly on the loading across the UD thickness. For the first time, the effect of the gradient of loading on the compressive strength of composites was demonstrated from a theoretical point of view.

In laminates made up with transverse plies, the key parameter is the combination of the number of consecutive 0° plies (thickness) with the gradient of loading across the laminate thickness. More precisely, it is the gradient of loading across the thickness of these contiguous plies that sets the transverse characteristic length of the phenomenon and therefore, it influences the mechanism under both pure compression and pure bending.

These results provide some clear explanations of the influence of the structure on the compressive strength. In order to draw definitive conclusions, further experimental investigations must be carried out, especially bending experiments on laminates are being achieved. Also, it would be interesting to predict both distribution and amplitudes of the fibre initial imperfection, the only parameter which is still not sufficiently known but was shown to control strongly the local plastic microbuckling mechanism. A comparison with experimental measurements must rely on such information that is hard to quantify today.

References

Anthoine-Rahier, O., Grandidier, J.C., Daridon, L., 1998. Pure compression testing of advanced fibre composites. Comp. Sci. Tech. 58 (5), 735–740.

Argon, A.S., 1972. Fracture of Composites. Treatise of Materials Science and Technology, vol. 1, Academic Press, New York.

Budiansky, B., 1983. Micromech. Comput. Struct. 16 (1), 3–12.

Budiansky, B., Fleck, N.A., 1993. Compressive failure of fiber composites. J. Mech. Phys. Solids 41 (1), 183–211.

Colvin, G.E., Swanson, S.R., 1993. In-situ compressive strength of carbon–epoxy AS4/3501-6 laminates. J. Engng. Mat. Tech. 115, 122–128.

Drapier S., Grandidier, J.-C., Gardin, C., Potier-Ferry, M., 1996. Structure effect and microbuckling. Special JNC9, Comp. Sci. Tech. 56, 861–867.

Drapier, S., Grandidier, J.-C., Gardin, C., Potier-Ferry, M., 1997. Theoretical study of structural effects on the compressive failure of laminate composites. Compt. Rend. de l'Acad. des Sci. Paris, Série II b 324, 219–227.

Drapier, S., Grandidier, J.-C., Potier-Ferry, M., 1999. Towards a numerical model of the compressive strength for long fibre composites. Eur. J. Mech/A Solids 18, 69–92.

Fleck, N.A., Deng, L., Budiansky, B., 1995a. Prediction of kink width in fiber composite. J. Appl. Mech. 62, 329–337.

Fleck, N.A., Shu, J.Y., 1995b. Microbuckle initiate in fibre composites: a finite element study. J. Appl. Mech. Phys. Solids 43 (12), 1887–1918.

Gardin, C., Potier-Ferry, M., 1992. Microflambage des fibres dans un matériau composite à fibres longues: analyse asymptotique 2-D. Compt. Rend. de l'Acad. des Sci. Paris, Série II 315, 1159–1164.

Grandidier, J.-C., Potier-Ferry, M., 1990. Microflambage des fibres dans un matériau composite à fibres longues. Compt. Rend. de l'Acad. des Sci. Paris, Série II 310, 1–6.

Grandidier, J.-C., Ferron, G., Potier-Ferry, M., 1992. Microbuckling and strength in long-fiber composites: theory and experiments. Int. J. Solids Struct. 29 (14/15), 1753–1761.

Grandsire-Vinçon, I., 1993. Compression des Composites Unidirectionnels: Méthodes d'Essais et Approche Micromécanique. Thèse de Doctorat de l'ENS Cachan.

Jochum, C., Grandidier, J.-C., Potier-Ferry, M., 1999. Modelling approach of microbuckling mechanism during cure in carbon/epoxy laminates. Proceedings of ICCM12, Paris, July 5–9, 1999.

Hutchinson, J.W., 1974. Plastic buckling. Adv. Appl. Mech. 14 (12), 67–144.

Kyriakides, S., Arseculeratne, R., Perry, E.J., Liechti, K.M., 1995. On the compressive failure of fiber reinforced composites. Int. J. Solids Struct. 32 (6/7), 689–738.

Paluch, B., 1994. Analyse des Imperfections Géométriques Affectant les Fibres dans un Matériau Composite à Renfort Unidirectionnel. La Recherche Aéronautique 6, 431–448.

Rosen, B.W., 1964. Mechanics of Composite Strengthening. Fibre Composite Materials, Am. Soc. Metals Seminar, Metal Parks, Ohio, 37–75.

Schaffers, W.J., 1977. Buckling in fiber reinforced elastomer. Text. Res. J. 502–512.

Swanson, S.R., 1992. A micro-mechanics model for in-situ compression strength of fiber composite laminates. ASME J. Engng. Mat. Technol. 114, 8–12.

t'Hart, W.J.G., Aoki, R., Bookholt, H., Curtis, P.T., Krober, I., Marks, N., Sigety, P., 1991. Garteur Compression Behaviour of Advanced CRFP. AGARD Report 785. The Utilisation of Advanced Composites in Military Aircraft. 73rd Meeting of the AGRAD Structures and Materials Panel held in San Diego, October 7–11.

Tvergaard, V., Needlemann, A., 1980. On the localization of buckling patterns. J. Appl. Mech. 47, 613–619.

Wisnom, M.R., 1991. The effect of the specimen size on the bending strength of unidirectional carbon fibre–epoxy. Comp. Struct. 18, 47–63.

Wisnom, M.R., 1992. On the high compressive strains achieved in bending tests on unidirectional carbon fibre/epoxy. Comp. Sci. Tech. 43, 229–235.

Wisnom, M.R., Atkinson, J.W., Jones, M.I., 1997. Reduction in compressive strain to failure of unidirectional carbon fibre–epoxy with increasing specimen size in pin-ended buckling tests. Comp. Sci. Tech. 57 (9/10), 1303–1308.